#738

SUBMITTED TO JOURNAL OF APPLIED PHYSICS
29/4/93

The Determination of Diffusion Profiles of Neodymium in Lithium Niobate by Means of Spatially-Resolved Fluorescence Measurements

Martin Hempstead

Optoelectronics Research Centre

University of Southampton

Southampton SO9 5NH

UK

Fax: 44 703 593149

We discuss the application of spatially-resolved measurements of fluorescence intensity to the determination of diffusion profiles, in this case of neodymium ions into lithium niobate, and to the concentration-dependence of the fluorescence lifetime. The technique permits a precise determination of diffusion depth, but extraction of detailed point-by-point concentration measurements is not possible. We give a detailed analysis of the effect on the accuracy of the method of systematic uncertainties, including quantum electrodynamical corrections and concentration-dependent lifetimes. The overall systematic error in measurement of diffusion coefficient is shown to be approximately 10%. The diffusion coefficients measured are consistent with previous values, but the fluorescence lifetimes obtained are significantly shorter than for bulk-doped Nd:$LiNbO_3$.

Introduction

The solid state system consisting of monocrystalline lithium niobate doped with neodymium ions has been exploited extensively since the first laser in this material was reported in 1967 [1]. Within the last few years, Q-switched and mode-locked waveguide lasers have been reported [2,3]. Until recently, all such devices were fabricated in lithium niobate doped from the melt with neodymium; an Nd:$LiNbO_3$ waveguide laser has now been reported into which the neodymium was introduced by diffusion [4]. Diffusion of rare earth ions into crystal substrates was pioneered by the fabrication of an Er:$LiNbO_3$ waveguide laser by this means [5], and has also recently been demonstrated for neodymium diffusion into lithium tantalate [6].

Design of the fabrication processes for such rare-earth-diffused waveguide devices requires knowledge of the diffusion coefficients and solubilities of the rare earth ions in the lithium niobate host. The calculation of diffusion profiles and times is sensitive to these parameters. Presently, the literature contains imprecise values of these parameters for neodymium [7] and rather more precise ones for erbium [7,8,9].

Three techniques have previously been applied to determination of the diffusion coefficients of rare earth ions in lithium niobate. Rutherford backscattering [RBS] has been employed for both the Er:$LiNbO_3$ and Nd:$LiNbO_3$ systems [7]. It has the disadvantages of limited sensitivity, relevant for the low maximum concentrations in the region of 0.2 at% obtaining in these systems, and limited depth range, in that the signal for backscattering from rare earth ions is swamped by background from the host crystal for depths greater than about 0.5 μm. Electron microprobe [EMP] analysis has been used

for the depth profiling of diffused erbium ions [8], and suffers from low sensitivity at the relevant concentrations. Secondary ion mass spectrometry [SIMS] has also been used for the determination of erbium depth profiles [9], and is extremely sensitive and accurate. However, it shares with the other two techniques the requirement for expensive equipment and the ability to provide information only about elemental composition, being insensitive, for example, to the valence state of the element.

In this paper, we describe the use of spatially-resolved measurements of fluorescence intensity to obtain information about the diffusion of neodymium into lithium niobate. This technique has several clear advantages over those described above. Since it is in principle a spectroscopic measurement, it can be made site- and valence-specific, although these potential virtues were not exploited in the present work. The time-dependence of the fluorescence can also be investigated, and in this paper we report measurements of fluorescence lifetimes as a function of dopant concentration in a diffused sample. Finally, spatially-resolved fluorescence measurement is relatively inexpensive, and utilizes apparatus likely to be available in any integrated optics laboratory. Similar techniques have been described in the literature, for the investigation of the erbium concentration distribution across an optical fiber preform [10] and in cytological investigations where the fluorescence is imaged and analyzed for intensity and lifetime in every pixel [11].

Principle of the measurement

In principle, by measuring the intensity of fluorescence emitted from a material under well-defined conditions of illumination with pump radiation, we measure the number of

fluorescing ions in the illuminated region. Fig. 1 illustrates the application of this principle to the determination of the concentration profile of neodymium diffused into lithium niobate. The shallow depth distribution is converted to an extended horizontal one by polishing a facet at a small angle to the initial surface. The pump beam is then focused and scanned across the polished facet to produce a fluorescence profile which may be converted to an integrated concentration profile.

In the 4-level Nd^{3+} system considered here, we measure the fluorescence emission in the region of 1084 nm from the $^4F_{3/2} \rightarrow {}^4I_{11/2}$ transition (although there is substantial fluorescence at vacuum wavelengths of 1300-1370 nm, and some in the 1800 nm region, the experiment described here was not sensitive to it). The fluorescence intensity is given by:

$$I_f = \varepsilon_{det} \times \frac{B_{rad}(\Omega)}{\tau_f} \times N h \nu_f \times \frac{I_p}{I_p + I_0} \qquad (1)$$

where I_0 is a constant with the dimensions of intensity, characteristic of the material and given by:

$$I_0 = \frac{h\nu_p}{\sigma_{abs}\tau_f} \qquad (2)$$

and: I_f, I_p are fluorescence and pump intensities, respectively

ν_f, ν_p are fluorescence and pump frequencies, respectively

τ_f is the fluorescence lifetime

σ_{abs} is the pump absorption cross section at ν_p

B_{rad} is the branching ratio for $^4F_{3/2} \rightarrow {}^4I_{11/2}$ radiative decay

Ω is the acceptance angle of the detection optics

ε_{det} is the detection efficiency of the photodiode

N is the Nd^{3+} concentration

Note that:

$$\tau_f = \frac{1}{\Gamma_{rad(\Omega)} + \Gamma_{rad(\overline{\Omega})} + \Gamma_{nrad}} \quad (3)$$

and:

$$B_{rad}(\Omega) = \Gamma_{rad(\Omega)} \tau_f \quad (4)$$

Here $\Gamma_{rad(\Omega)}$ and $\Gamma_{rad(\overline{\Omega})}$ are the radiative widths inside and outside the detector acceptance angle, and Γ_{nrad} is the "non-radiative" width (throughout this paper, non-radiative decays will be taken to include radiative decays outside 1060-1110 nm). In eq. 1, we have assumed that an ion excited by pump absorption to the highest energy state is immediately de-excited by non-radiative phonon emission to the $^4F_{3/2}$ state, and that an ion in the $^4I_{11/2}$ state is immediately returned to the system ground state by phonon de-excitation. Thus, all else being equal, fluorescence intensity is proportional to the number of fluorescing ions in the illuminated region.

Depth profiling from fluorescence intensity measurements has the disadvantage that the direct result is an integrated concentration distribution, which reduces sensitivity to departures from Fick's law.

Potential Sources of Systematic Error

In order to be able to interpret fluorescence intensity as proportional to the number of ions

under illumination, we must be confident that all other quantities in eq. 1 are independent of concentration. This need not necessarily be the case. I_p and ν_p are determined by experimental conditions, but the remaining quantities may well be sensitive to concentration, through the effects of crystal strain, refractive index changes and ion-ion interactions.

Crystal strain may arise as the neodymium diffuses into the lattice, since the size of the neodymium ion (0.099 nm) is larger than the size of the niobium (0.069 nm) or lithium ion (0.068 nm) it replaces [12]. The typical maximum neodymium ion concentration is 0.2 at %, so the average strain introduced into the crystal is unlikely greatly to exceed $2x10^{-4}$.

The spectral distribution of ν_f in neodymium-diffused $LiNbO_3$, which determines ε_{det}, is not distinguishable from that of the bulk-doped material [4], but may in fact vary with the crystal strain [13]. We can estimate the magnitude of this effect by noting that a similar strain along the x-axis would be induced by an approximately 10 K temperature rise [14]. Ref. 13 contains spectra for Nd:$LiNbO_3$ at 77 K and 295 K, which show a relative thermal shift in average emission wavelength of 2 nm and 5 nm for π- and σ-polarized emission respectively. The detector response is approximately a linear function of wavelength from 1050 (ε_{det}=1.0 a.u.) to 1110 nm (ε_{det}=0.4 a.u.), so the signal measured for a constant photon flux is dependent upon the average emission wavelength. Scaling for a 10 K temperature change, we find less than 0.5% change in detected fluorescence signal.

The pump absorption cross section σ_{abs} will also be dependent upon changes in the crystal

field, and may in principle be estimated from the saturation behavior of the fluorescence. We have no information on its variation with concentration, but in view of the small strains involved and the small variations in the emission spectrum discussed above, we consider its effect to be negligible.

If all other factors are held constant, Γ_{rad} is scaled by a factor f_n which depends upon the host refractive index according to the local field correction [15]:

$$f_n = \frac{n(n^2+2)^2}{9} \tag{5}$$

Variations in refractive index may arise from the neodymium dopant, or from the photorefractive effect. In fact, the maximum index change arising from the former cause is likely to be less than 5×10^{-3} (the index change from Ti^{4+} doping at similar concentrations [16]) and from the latter less than 10^{-3} [17]. This leads to a change in Γ_{rad} of less than about 1%. Γ_{rad} will also change with variations in the crystal field.

Γ_{nrad} for neodymium is dominated by the ion-ion interactions known as concentration-quenching, in which part of the excitation energy is non-radiatively transferred from one ion to another. This effect should be proportional to N^{α}, where $1\leq\alpha\leq2$ for randomly distributed ions [18]. Some indication of the magnitude of the variations in Γ_{rad} and Γ_{nrad} is obtained below, using depth-dependent lifetime measurements. There are also depth-dependent modifications to Γ_{rad} and $B_{rad}(\Omega)$ arising from the effect of a dielectric boundary on the vacuum fluctuation intensity. These are discussed in more detail below.

Quantum electrodynamical variations in spontaneous emission rates

The spontaneous emission rate of a dipole is proportional to the mean square fluctuation in the vacuum electric field component parallel to the dipole. In free space, or in the depths of a dielectric, this quantity is independent of polarization and position, but near the boundary of a dielectric it becomes strongly dependent upon both factors [19], to the extent that for a host material such as $LiNbO_3$ with a refractive index of 2.2 and for polarization perpendicular to the surface, the spontaneous emission rate can be below bulk values by over 30% within $\lambda/4$ of the surface (fig.2).

A similar effect will prevail for waveguide structures, with the precise details depending upon the modal spectrum. The modification of the spontaneous emission rate has consequences for the behavior of waveguide lasers and optical amplifiers. For the present application, it will give rise to a position-dependent radiative emission rate.

In order to model the quantum electrodynamical (QED) corrections to the present measurement, it is necessary to specify the illumination and observation conditions. We assume the illumination is a Gaussian beam of low intensity (so that the absorption is far from saturation). Under this condition, the total fluorescence rate will be approximately independent of τ_f, but will be distributed among the different dipole moments according to the QED calculations. We will take the detected fluorescence to be that emitted normal to the surface, in this case a yz face of the crystal. The fluorescence spectrum of room-temperature Nd:$LiNbO_3$ [14] may be taken to be radiated by dipoles along the x, y and z axes, with the x- and y-oriented dipoles identical and the total magnitude of emission in the bulk host approximately the same for each direction, assuming that the detector is

uniformly sensitive to all emission wavelengths from 1060 nm to 1110 nm. We model $LiNbO_3$ as an isotropic material with a refractive index of 2.2, and ignore the effect of the QED modulation of the 1300 nm fluorescence band, which has a length scale 20% greater.

The QED corrections are then calculated from the convolution, as functions of depth, of the fraction of fluorescence emitted by the y- and z-dipoles with the concentration distribution produced by the diffusion process;

$$F(x) = \int_x^\infty C(x')Q(x'-x)dx' \tag{6}$$

where:

F(x) is proportional to the fluorescence intensity

x is the depth of the polished surface below the original one at the pump beam spot

$C(\chi)$ is the concentration of fluorescing ions at depth χ below the original surface

$Q(\zeta)$ is the QED correction factor at depth ζ below the new surface

In practice, the concentration profiles resemble a complementary error function (ERFC) or a Gaussian distribution. For an ERFC profile the result, following ref. 19, is shown in fig. 3, for the two extreme cases of (i) negligible non-radiative and (ii) negligible radiative contribution to the lifetime, and it is immediately obvious that there is a definite difference between uncorrected and QED-corrected distributions. We obtain the apparent diffusion depth by fitting the QED-corrected fluorescence profiles to an integrated ERFC, where the adjustable parameters are the intensity and depth scales. The results are shown in table I for different diffusion depths. The greatest variation is in the fluorescence intensity scale, but a depth correction of up to 2% is required (which implies a 4% correction to the inferred diffusion coefficient); in both cases, the corrected distributions are well fitted by

the complementary error function. A similar pattern is seen for a half-Gaussian diffusion distribution; in this case the results of fitting with an integrated Gaussian of adjustable amplitude and width are listed in table I.

Only an extremely accurate measurement of the integrated concentration profile can reveal the small deviations introduced by the QED corrections. Note that this would not be the case with the profiles obtainable by ion implantation, which can produce sub-surface layers of rare-earth ions of thickness rather less than the fluorescence wavelength [7]. A fluorescence scan across an angle-cut surface could over a certain depth range show an *increase* of intensity with depth.

Sample Preparation

The samples used for this study were taken from x-cut slices of dimensions 50x50x1 mm^3 of undoped lithium niobate supplied by Fujian Castech of China. They were produced in the course of fabricating an Nd:$LiNbO_3$ waveguide laser [4], and were therefore not optimized for the measurement of diffusion coefficients. The conditions of neodymium diffusion are given in table II; note that each sample was subjected to diffusions at two temperatures. For sample A, sufficient neodymium was deposited initially that the diffusion certainly did not exhaust the source, whereas for sample B, the source was exhausted during the first part of the second diffusion stage.

Fragments of samples A and B were prepared for the fluorescence measurement by polishing a face at a shallow angle (approximately 1:100) to cut into the diffused surface.

To achieve this, the sample was mounted on a jig at an angle of about 0.5° to the polishing plate. It was lapped on an iron plate with a 9 μm and then a 3 μm alumina slurry, then polished with an aqueous suspension of silica on an aluminum plate with a polyurethane coating.

To facilitate analysis of the results of the fluorescence measurement, it is desirable that the transition region between the original and polished faces be as sharp as possible. When a facet is polished nearly parallel to the initial face, the boundary between the two surfaces tends to be indistinct, with a slow curvature from one to the other. The smaller the angle, the more severe this effect. With sample A an attempt to obtain a sharp transition was made by protecting the original face with a sacrificial layer of lithium niobate glued on with about 1 μm thickness of epoxy. The surface profile shown in fig. 4(a) was obtained, where the transition region occupies about 0.5 μm in depth. This particular technique was limited by the adhesion and hardness of the epoxy, which tended to break off near the edge leaving it exposed to rounding by the polishing. With sample B, an improvement on this was made using a sacrificial layer of copper oxide (CuO). This was deposited by vacuum evaporation of CuO powder; the reduction observed was then reversed by annealing in air at 250°C for several days. The use of CuO was motivated by its hardness and melting point, which at approximately 4 on Moh's scale and 1326°C respectively are close to those of $LiNbO_3$ (5 and 1253°C respectively). Thus whether polishing is a grinding or melting process [20], CuO and $LiNbO_3$ should behave in a similar fashion. Moreover, both being oxides it was expected that they might bond well. Using this approach, the profile of fig. 4(b) was generated. Note that the angle of polish is the same as for sample A, but that the depth of the transition region is half as deep, at about .25

μm. Since these samples were prepared, we have been informed of several polishing procedures that may work equally well [8, 21-23].

The spatial resolution of this technique is limited not only by the size of the focused pump beam spot but also by the surface quality. The roughness of the initial and final surfaces introduces a depth error of about 10 nm, with undulations over periods of tens of microns; unmeasured differences between initial and final curvatures are estimated - from a measurement of the curvature of the remaining initial diffused surface - to introduce slowly varying "systematic" differences between true and measured depth of approximately 30 nm.

Modelling the Concentration Distributions

The expected dopant distributions were modelled using the figures in ref. 7, and assuming a simple diffusion equation:

$$D\frac{\partial^2 C}{\partial x^2}=\frac{\partial C}{\partial t} \quad \text{for } x>0,\ t>0 \tag{7}$$

with boundary conditions of:

$$C(0,t)=C_{max} \quad \text{for } t>0 \tag{8}$$

$$C(x,0)=0 \quad \text{for } x>0 \tag{9}$$

where C_{max} is the solubility limit, which is temperature-dependent, as detailed in ref. 7.

For source-free diffusion, boundary condition (8) is replaced by:

The solutions to the diffusion equation for the different conditions are:

$$\frac{\partial C}{\partial x}=0 \quad \text{at } x=0,\ t>0 \tag{10}$$

(1) For diffusion from infinite source at x=0 with maximum concentration C_{max} and diffusion coefficient D:

$$C(x,t)=C_{max}\text{erfc}\left[\frac{x}{\sqrt{2Dt}}\right] \quad \text{for } x>0 \tag{11}$$

where "erfc" represents the complementary error function.

(2) For diffusion from infinite source at x=0 at temperature T_1 for time t_1 and then higher temperature T_2 for time t_2 (assuming $C_{max}(T_2)>C_{max}(T_1)$):

$$C(x,t_1+t_2)=C_{max}(T_1)\text{erfc}\left[\frac{x}{\sqrt{2D_1t_1+2D_2t_2}}\right] +(C_{max}(T_2)-C_{max}(T_1))\text{erfc}\left[\frac{x}{\sqrt{2D_2t_2}}\right] \quad \text{for } x>0 \tag{12}$$

(3) For diffusion from source at temperature T_1 for time t_1, for time t_2 at temperature T_2 until source exhausted, then at the same temperature for time t_3 to relax concentration distribution:

$$C(x,t_1+t_2+t_3)=\int_{-\infty}^{\infty}C_0(x',t_1+t_2)\frac{e^{-\frac{(x-x')^2}{4D_2t_3}}}{\sqrt{4\pi D_2t_3}}dx' \tag{13}$$

where $C_0(x',t_1+t_2)$ is given by equation 12 for x>0 and:

$$C_0(-x,t)=C_0(x,t) \tag{14}$$

Table III lists the parameters of the concentration distribution estimated from ref. 7 for

each of sample A and B, and numerical simulations are shown in fig. 5. The expected distribution for sample A is approximately a complementary error function, whereas for sample B it more closely resembles a Gaussian distribution.

Fluorescence Intensity Measurements

Fig. 6 shows a schematic diagram of the apparatus used for measuring the fluorescence intensity as a function of position. Two positions for the fluorescence detector, labeled "reflection" and "transmission" in fig.6, were used.

Illumination was provided by a Ti:sapphire laser, pumped by an Argon ion laser. It was operated in the wavelength range 790 nm to 840 nm, and produced a maximum output power at 814 nm of about 300 mW. An isolator was placed at the output of the Ti:sapphire laser, causing a polarization rotation to a position halfway between the y and z axes of the substrate. The output intensity was found to be very unstable, varying by a factor of 2 in instantaneous power over a period of seconds and in average power by tens of percent over minutes. This was a problem for the present measurements, which took place over an hour or more. To remedy this, the fluorescence was not measured directly, but divided by a signal proportional to the sum of the pump power measured in the photodiode PD1 and an offset. The offset was required because the fluorescence signal was somewhat saturated, and not directly proportional to the pump power; the offset magnitude was adjusted until variations in the pump power produced no variation in normalized fluorescence signal as indicated on an oscilloscope.

In order that the entire depth of Nd-diffused $LiNbO_3$ be exposed uniformly and to achieve a good transverse spatial resolution for the measurement, the pump beam was focused to a spot about 5 μm in radius by a 10x microscope objective lens (N.A.=0.25). A Gaussian beam of this waist size produces a beam divergence of 50% in 75 μm of lithium niobate, giving insignificant spreading in a diffused layer of the order of only 10 μm deep. Beam divergence is relevant only if the fluorescence is not far from saturation, since away from saturation the fluorescence power depends only upon the total pump power (in this case, the ultimate spatial resolution for a pump beam at 810 nm through a 10 μm-thick layer in lithium niobate is about 1.5 μm, with the peak intensity of the focused spot varying by a factor of 2 through the layer). Illumination was incident from air onto the diffused surface, to ensure that back reflections - traveling through 2 mm of lithium niobate - would be sufficiently attenuated by beam spreading to avoid uneven intensity distribution through interference.

For the intensity measurements, the fluorescence emitted was collected in the "reflection" configuration; thus there was no interference between the fluorescing source and its 14% reflection at the lithium niobate/air boundary as would be the case with the "transmission" configuration. The "field volume" of the fluorescence-collection optics was verified to cover the entire emitting region.

Pump light was filtered from the signal by long-wavelength pass filters, which also removed approximately 60% of the fluorescence power. Normalized fluorescence intensity measurements were obtained by reading the amplitude of the chopped pulses from a Tektronix 2430A digital storage scope averaging over 256 traces. In the case of the

lifetime measurements, the data were collected in the transmission configuration, in order that the fluorescence not be cut off by the chopper.

The sample was supported on a mount with manual micrometer operation of 2 translational and 2 rotational degrees of freedom. It was necessary to align the sample carefully, so that the pump beam remained sufficiently in focus over the entire scan of 1-2 mm. The video camera was used to image the diffused surface to permit alignment and focusing. The scan was performed by moving the sample horizontally transverse to the laser beam. For convenience in matching depth and fluorescence scans, it was arranged that the scan ran parallel to and between the titanium stripes formed on samples A and B for waveguide fabrication. The accuracy of the table motion was checked using a sample ruled with lines spaced every 100 μm, and found to be linear and correctly scaled to within a few tenths of a percent.

In order to match the fluorescence measurements to a depth, a surface profile was obtained using a Tencor Alphastep mechanical surface profiler. The starting point for the scan was indicated by a slight optical aberration where the crystal had been photorefractively altered by the pump beam. Orientation of this trace to the fluorescence scan was possible to a negligible error of a fraction of a degree, but the starting position was subject to an error of approximately 10 μm both along and perpendicular to the scan, equivalent to a depth uncertainty of 100 nm for sample B. This difficulty could have been avoided with photolithographic reference marks. The reference level of the unpolished surface was judged by eye from the trace, with an effective slope error, and hence distance/depth conversion error, estimated to be about 0.5%. Depths were read from the trace, at the

positions for which fluorescence measurements were made.

Results

Fig. 7 shows the data for fluorescence vs. scan position. Note that the measurements are almost background-free, but rather noisy. Fig. 8 shows fluorescence vs. depth profiles. It will be noted that for sample B there are gentle fluctuations which are probably due not to real structure in the concentration distribution but rather to substantial variations in average Ti:sapphire output power over the course of the data collection. This variation is demonstrated by the different fluorescence intensities shown in fig. 8(b) when at the end of the scan the laser spot was backtracked to previously measured positions. The effect of pump instability can be reduced by multiple scans.

Due to the complicated thermal history of the samples, it is difficult to obtain accurate estimates of the parameters involved, since their covariance matrices are far from diagonal.

There are three independent parameters for Nd(40); the diffusion coefficients at the two temperatures involved and the ratio R of the maximum concentrations. Values of R were chosen in the range 1.-2.5 and the data then fitted to the function given in eq. 12. The relative scaling of the two terms was calculated from the value of R, and the fitted parameters were an overall normalization and depth scaling factors for the two error functions. From the scaling factors and the times for each diffusion stage, the diffusion coefficients were extracted according to eq. 12. The best fit is shown in fig. 8(a). The average of the two values of the diffusion coefficient shows substantially smaller variation

than the individual values, and is the diffusion coefficient at some intermediate temperature. We therefore quote $D=1.4\pm.4\times10^{-14}$ cm^2 s^{-1} for the diffusion coefficient of neodymium into lithium niobate at T=1275±10 K. The statistical error, for the depth scaling when fitting to a single error function, is 3%. This represents the intrinsic statistical accuracy of the data for a single scan, and would give an error of 6% for the diffusion coefficient for a sample diffused at a similar, single, temperature.

In the case of Nd(200) there are 4 independent parameters; these are the maximum concentration and diffusion coefficient at each temperature. The presence of an integral in the general solution (eq. 13) causes problems with direct fitting for the parameters, so an approach was adopted in which 3 parameters were fixed and the fourth varied until a model distribution was generated [according to eqs. 7-14] which matched the experimental one in depth scale. The best fit is shown in fig. 8(b). The goodness-of-fit was not very sensitive to the model parameters, which leads to a large systematic error in the estimate of any one parameter, due to the non-diagonal nature of the covariance matrix. We thus extract the result that $D=4\pm1\times10^{-14}$ cm^2 s^{-1} at T=1340±5 K.

Fig. 9 shows the results of the present investigation compared to previous measurements [7]. Taking into account the fact that we used x-cut rather than z-cut material, our results appear consistent with those of ref. 7, indicating that the diffusion rate along the x-axis is comparable to that along the z-axis.

Lifetime measurements

Lifetime measurements were made at various points along the depth scan, in the transmission configuration, by chopping the pump light and observing the decay of the fluorescence signal on the oscilloscope. Readings were taken from the scope and fitted to an exponential function to obtain the lifetime. The first 100 μs after the chopped pump were ignored to avoid the trailing edge of the pump pulse. Modelling indicates that the value obtained in this way for a population of ions with lifetimes varying by ±10% will, to a very good approximation, be the average lifetime of the ensemble. Fig. 10 shows the data and fitted decay curves, and fig. 11 shows the inverse of fluorescence lifetime as a function of average concentration for sample B. The average concentration was estimated from the distribution obtained from the model that best fit the data, and from the assumption that all the deposited neodymium (2.0±0.2 μg cm^{-2}) was diffused into the sample. The concentration of sample A was not known in absolute figures, but lifetimes of 102±3 μs and 111±5 μs were measured for average concentrations of $0.6C_{max}$ and $0.2C_{max}$ respectively.

It will be seen that there is a trend to shorter lifetimes at higher concentrations, consistent with concentration quenching. Previously published lifetimes [24-26] are also shown on fig. 11, and are significantly higher than those measured in our samples. This may be due to strain in the diffused crystals, leading to a distortion of the crystal field and a consequent increase in radiative rate, or a greater non-radiative coupling if the neodymium is less uniformly distributed than in the melt crystals, perhaps being concentrated at dislocations. A further possibility is that the excitation energy is trapped in defects in the crystal as it migrates between neodymium ions before emission in fluorescence decay.

One mechanism for such trapping consists in rare-earth impurities, perhaps dysprosium, which could resonantly absorb the excitation energy and lose it through rapid, cascading non-radiative decays. The neodymium used is specified as 99.9% pure, being unlikely to contain more than 100 ppm of any single lanthanide contaminant. Estimating the diffusion chain for the excitation energy to cover about 100 neodymium ions [18], we find that an introduced impurity trap concentration of 0.2% of the rare-earth ions would be required for the observed lifetime reduction through a 20% non-radiative decay branching ratio.

Correction of Fluorescence Depth-Profiling for Concentration-Dependent Lifetime

The observed lifetime variations probably indicate a change in the relative contributions of radiative and non-radiative decays to the fluorescence lifetime. They must therefore be considered when analyzing the fluorescence depth profile as an indication of concentration. The details of the correction depend upon the balance between radiative and non-radiative decay paths. At Nd^{3+} concentrations similar to those we investigated, neodymium-doped aluminosilicate fibers show little concentration-quenching effect [27], and a fluorescence lifetime remarkably similar to that in lithium niobate if the local field correction, eq. (5), is made. We may conclude that the maximum lifetime seen, 120 μs [24], represents an almost unquenched decay of the excited state. The lifetime in excess of 90 μs seen in our diffused samples then indicates a radiative quantum efficiency above 75%. In this case, the largest correction factor arises if the change in lifetime is entirely due to changes in the non-radiative cross-section. Then the fluorescence intensity, for constant absorption cross section and weak pumping, will be proportional to the lifetime, and the fluorescence-depth profile will be deeper than the concentration profile, since high-concentration regions, with

shorter lifetimes, will have relatively suppressed fluorescence. Fitting the lifetime data to a linear function of concentration, we have examined the effect of correcting the fluorescence intensity in our models to account for the lifetime-dependence, and found the corrected fluorescence intensity distribution to have a depth about 2% greater than the concentration distribution, requiring a 5% correction to the inferred diffusion coefficient.

Accuracy of the Present Method for Measurement of Diffusion Coefficient

Although the diffusion coefficients measured above have substantial errors, these are not intrinsic to the measurement, and samples prepared specifically for the measurement of diffusion coefficient would have statistical errors of 2.5% or less from the analysis of a single scan. The correction factors for the concentration-dependence of the lifetime and QED effects make the greatest contributions to the systematic error, each having an estimated uncertainty of 5% or less.

Calibration of the fluorescence signal

The measurements described here have indicated only relative quantities of fluorescent ions as the pump beam is scanned along the profile; absolute measurements require a calibration sample of known concentration, and, ideally, of a distribution similar to the diffusion profiles under measurement. This latter requirement arises from the QED and lifetime corrections, which are the most significant sources of systematic uncertainty in calibrating the fluorescence intensity and which depend upon the distribution. Without correction, this would - for Nd:$LiNbO_3$ - lead to a 20% uncertainty in scaling from the calibrated sample to the test sample, as may be seen from table I. Once the test sample

distribution is known, a much more accurate calibration scaling can be modeled, and the remaining uncertainty is due to the other concentration-dependent effects discussed above. The sample must not fluoresce in regions outside the effective "depth-of-field" of the apparatus, which in practice in the present system means more than 10 μm deep.

Conclusion

We conclude that measurement of diffusion coefficient by means of spatially resolved fluorescence is a simple, inexpensive and accurate technique, provided that the sample may be prepared with a shallow wedge polish, and that the fluorescing system emits sufficient light to be readily detected. Obtaining concentration profiles from the fluorescence intensity distribution is complicated by the effect of QED effects and concentration-dependent lifetimes which change the spontaneous emission rate; these effects may however to some extent be taken into account. The resolution of the method can be as good as 30nm of depth with the solid-state system described above. A fundamental limit to the measurement of concentration by fluorescence intensity is set by uncertainty about the relationship between the two - in the present case, concentration-dependent lifetimes and QED effects introduce a systematic error of about 5% in the measurement of diffusion coefficient. Using the method we have obtained diffusion depths consistent with previous measurements. We have also shown that the fluorescence lifetime is shorter in neodymium-diffused than in bulk-doped lithium niobate, and that the lifetime exhibits weak concentration dependence.

Acknowledgements

The author acknowledges useful discussions with J.S. Wilkinson and W.S. Brocklesby. This work was supported through sponsorship of the Optoelectronics Research Centre by the UK Science and Engineering Research Council.

REFERENCES

1. N.F. Evlanova, A.S. Kovalev, V.A. Koptsik, L.S. Kornienko, L.N. Rashkovich, "Stimulated Emission of $LiNbO_3$ Crystals with Neodymium Impurity," JETP Lett., **5**, 291-293, 1967.

2. E. Lallier, J.-P. Pocholle, M. Papuchon, Q. He, M. De Micheli, D.B. Ostrowsky, "Integrated Q-Switched Nd:MgO:$LiNbO_3$ Waveguide Laser," Electron. Lett., **28**, 1428-1429, 1992.

3. E. Lallier, J.-P. Pocholle, M. Papuchon, Q. He, M. De Micheli, D.B. Ostrowsky, C. Grezes-Besset, E. Pelletier, "Integrated Nd:MgO:$LiNbO_3$ Mode-Locked Waveguide Laser," Electron. Lett., **27**, 936-937, 1991.

4. M. Hempstead, J.S. Wilkinson, L. Reekie, "Waveguide Lasers Operating at 1084 nm in Neodymium-Diffused Lithium Niobate," IEEE Photonics Technology Letts., **4**, 852-855, 1992.

5. R. Brinkmann, W. Sohler, H. Suche, "Continuous-Wave Erbium-Diffused $LiNbO_3$ Waveguide Laser," Electron. Lett., **27**, 415-417, 1991.

6. N.A. Sanford, J.A. Aust, K.J. Malone, D.R. Larson, A. Roshko, "Nd:$LiTaO_3$ Waveguide Laser," Optics Lett., **17**, 1578-1580, 1992.

7. Ch. Buchal, S. Mohr, "Ion Implantation, diffusion and solubility of Nd and Er in $LiNbO_3$," J. Mater. Res., **6**, 134-137, 1991.

8. D.M. Gill, A. Judy, L. McCaughan, J.C. Wright, "Method for the Local Incorporation of Er into $LiNbO_3$ guided wave optic devices by Ti co-diffusion," Appl. Phys. Lett., **60**, 1067-69, 1992.

9. M. Fleuster, Ch. Buchal, H. Holzbrecher, U. Breuer, M. Dinand, H. Suche, R. Brinkmann, W. Sohler, "Mev Ion Implantation of Er into $LiNbO_3$," presented at Materials

Research Society Fall Meeting 1992, to be published in Mat. Res. Soc. Sym. Proc. (1993).

10. J.F. Marcerou, B. Jacquier, A.M. Briançon, J.C. Gâcon, H. Fevrier, J. Augé, "Rare Earth Concentration and Localization in Nd^{3+} and Er^{3+}-doped fibre amplifiers," J. Luminescence, **45**, 108-110, 1990.

11. J.R. Lakowicz, "Fluorescence Lifetime Sensing Generates Cell Images," Laser Focus World, May 1992, 60-80.

12. C.R.C. Handbook of Chemistry and Physics, 68th edition, ed. R.C. Weast, F-159.

13. L.F. Johnson, A.A. Ballman, "Coherent Emission from Rare Earth Ions in Electro-Optic Crystals," J. Appl. Phys., **40**, 297-302, 1969.

14. S.C. Abrahams, H.J. Levinstein, J.M. Reddy, "Ferroelectric Lithium Niobate. 5. Polycrystal X-ray Diffraction Study between 24° and 1200°C," J. Phys. Chem. Solids, **27**, 1019-1026, 1966.

15. N.Q. Chako, "Absorption of Light in Organic Compounds," J. Chem. Phys., **2**, 644-653, 1934.

16. R.V. Schmidt, I.P. Kaminow, "Metal-diffused optical waveguides in $LiNbO_3$," Appl. Phys. Lett., **25**, 458-460, 1974.

17. A.M. Glass, "The Photorefractive Effect," Opt. Eng., **17**, 470-479, 1978.

18. H.G. Danielmeyer, M. Blätte, P. Balmer, "Fluorescence Quenching in Nd:YAG," Appl. Phys., **1**, 269-274, 1973.

19. H. Khosravi, R. Loudon, "Vacuum Field Fluctuations and Spontaneous Emission in the Vicinity of a Dielectric Surface," Proc. R. Soc. Lond. A, **433**, 337-352, 1991.

20. F. Twyman, "Prism and Lens Making," Chapter 3, 2nd Edition, 1952, pub. A. Hilger.

21. N.A. Sanford, private communication.

22. D.M. Gill, private communication.

23. J. Steffen, A. Neyer, E. Voges, N. Hecking, "Refractive Index Profile Measurement Techniques by Reflectivity Profiling: Vidicon Imaging, Beam Scanning and Sample Scanning," Appl. Optics, **29**, 4468-4472, 1990.

24. T.Y. Fan, A. Cordova-Plaza, M.J.F. Digonnet, R.L. Byer, H.J. Shaw, "Nd:MgO:$LiNbO_3$ Spectroscopy and Laser Devices," J. Opt. Soc. Am., **3**, 140-147, 1986.

25. L.I. Ivleva, A.A. Kaminskii, Y.S. Kuz'minov, V.N. Shpakov, "Absorption, Luminescence and Induced Emission of $LiNbO_3$-Nd^{3+} Crystals," Sov. Phys. Dokl., **13**, 1185, 1969.

26. I.P. Kaminow, L.W. Stultz, "Nd:$LiNbO_3$ Laser," IEEE J. Quant. Elect., QE-11, **306** (1975).

27. P.L. Scrivener, P.D. Maton, A.P. Appleyard, E.J. Tarbox, "Fabrication and Properties of Large Core, high NA, High Nd^{3+} Content Multimode Optical Fibers for Temperature Sensor Applications," Electron. Lett., **26**, 872-873, 1990.

LIST OF TABLES

I. Comparison of apparent diffusion depths for model fluorescence intensity distributions generated with and without QED corrections as discussed in the text.

II. Fabrication conditions for samples of diffused Nd:$LiNbO_3$. Temperature uncertainty 5 K; duration uncertainty 0.25 hour.

III. Parameters of model Nd concentration distribution for Nd:$LiNbO_3$ samples.

LIST OF FIGURES

1. Principle of the Spatially-Resolved Fluorescence Measurement.

2. QED corrections as a function of distance into a high-index dielectric material from boundary with vacuum: magnitude of vacuum fluctuations relative to vacuum value, parallel (1) and perpendicular (2) to dielectric boundary. Curve (3) shows spontaneous emission rate into vacuum normal to boundary, normalized to bulk value.

3. Effect of QED corrections on fluorescence intensity distribution for complementary error function (erfc) diffusion profile. Inset shows the difference between corrected and uncorrected distributions.

4. Surface profiles of samples A and B after preparation of the angle-polished facet, as measured with Tencor Alphastep.

5. Modeled neodymium concentration profiles based on parameters in table III.

6. Apparatus for spatially-resolved fluorescence measurement (schematic). Boxes with broken border indicate position of signal detection optics in "reflection" and "transmission" configurations.

PL: Ti:sapphire pump laser

ISO: optical isolator

FF: fluorescence filter

DM: dichroic mirror (R_{max} at 1064 nm)

L: 10x objective lens

PH: pinhole

VC: silicon vidicon

C: mechanical chopper

PF: pump filter set

SPD: signal-detection photodiode

PPD: pump-detection photodiode

7. Fluorescence intensity against scan position.

8. Fluorescence against depth, with best fit model shown.

9. Comparison of present measurements of diffusion coefficient with those of ref. 7

10. Decay of fluorescence decay with time. The data are fit to an exponential decay plus an offset. Note that each data set is on its own scale of fluorescence signal.

11. Lifetime as a function of average Nd^{3+} concentration. Note that previous measurements are for bulk-doped samples, and those from ref. 24 are for Nd:MgO:$LiNbO_3$.

Diffusion depth (μm)	Fitted Depth (μm); Maximum fluorescence intensity		
	Uncorrected	QED correction (i)	QED correction (ii)
Complementary Error Function Concentration Distribution			
0.50	0.50; 1.00	0.51; 1.22	0.51; 1.00
1.00	1.00; 1.00	1.02; 1.12	1.01; 0.99
2.50	2.50; 1.00	2.53; 1.05	2.50; 0.99
Gaussian Concentration Distribution			
0.50	0.50; 1.00	0.52; 1.18	0.51; 0.99
1.00	1.01; 1.00	1.03; 1.09	1.01; 0.98
2.50	2.49; 1.00	2.53; 1.04	2.48; 0.99

Table I

Comparison of apparent diffusion depths for model fluorescence intensity distributions generated with and without QED corrections as discussed in the text.

Sample A Nd thickness approximately 40 nm; dry O_2 atmosphere		
Nd diffusion	40 hours	1270 K
Ti stripe diffusion	9 hours	1280 K
Sample B Nd thickness approximately $2x10^{-6}$ g cm^{-2}; dry O_2 atmosphere		
Nd diffusion	203 hours	1290 K
Nd diffusion	210 hours	1340 K

Table II

Fabrication conditions for samples of diffused Nd:$LiNbO_3$. Temperature uncertainty 5 K; duration uncertainty 0.25 hour.

Sample		Temp K	Time hr	C_{max}/ (10^{-2} g cm^{-2})	D/ (10^{-14} cm^2 s^{-1})
A	Diffusion from surface layer	1270	40	0.4	0.7
		1280	9	0.6	1.0
B	Diffusion from surface layer	1290	203	0.9	1.4
		1340	11	2.2	7.6
	Source-free diffusion	1340	199	2.2	7.6

Table III

Parameters of model Nd concentration distribution for Nd:$LiNbO_3$ samples.

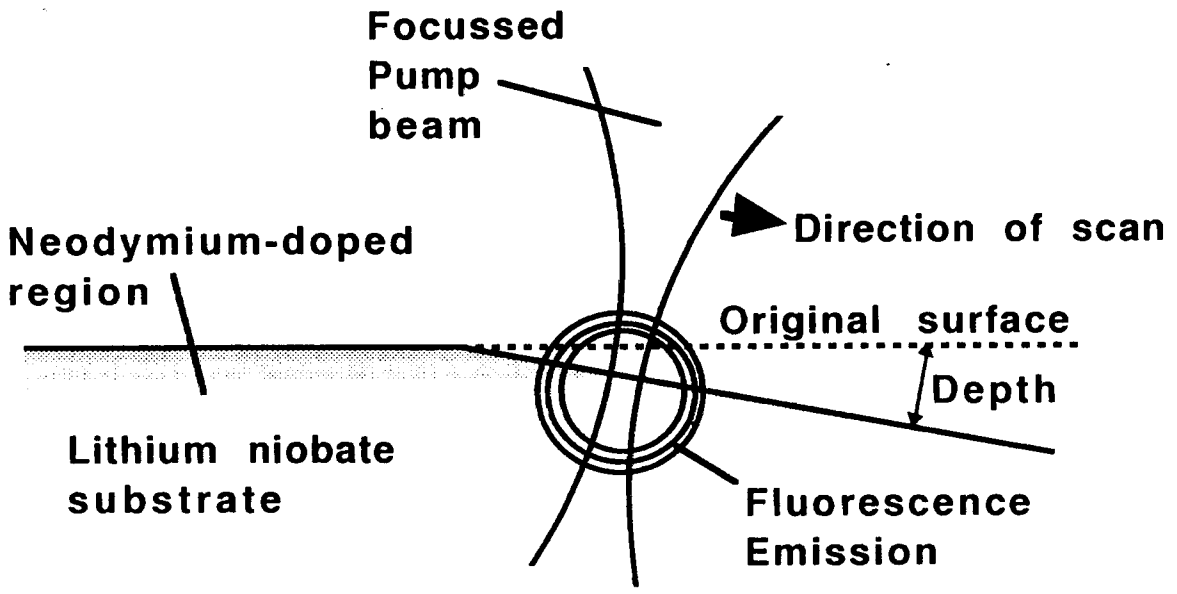
Focussed
Pump
beam
Direction of scan
Neodymium-doped
region
Original surface
Depth
Lithium niobate
substrate
Fluorescence
Emission

FIGURE 1.

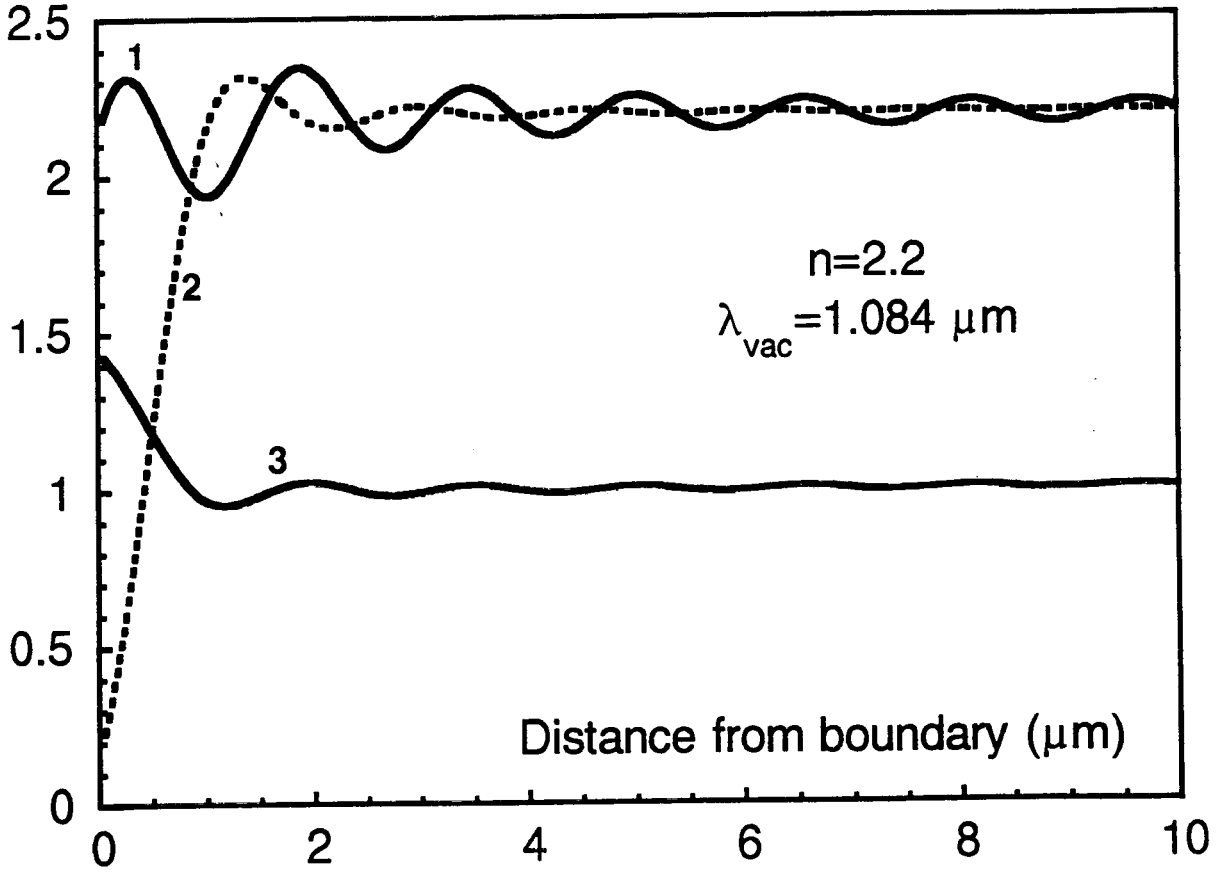
2.5
2
1.5
1
0.5
0
0
2
4
6
8
10
1
2
3
n=2.2
λvac=1.084 μm
Distance from boundary (μm)

FIGURE 2

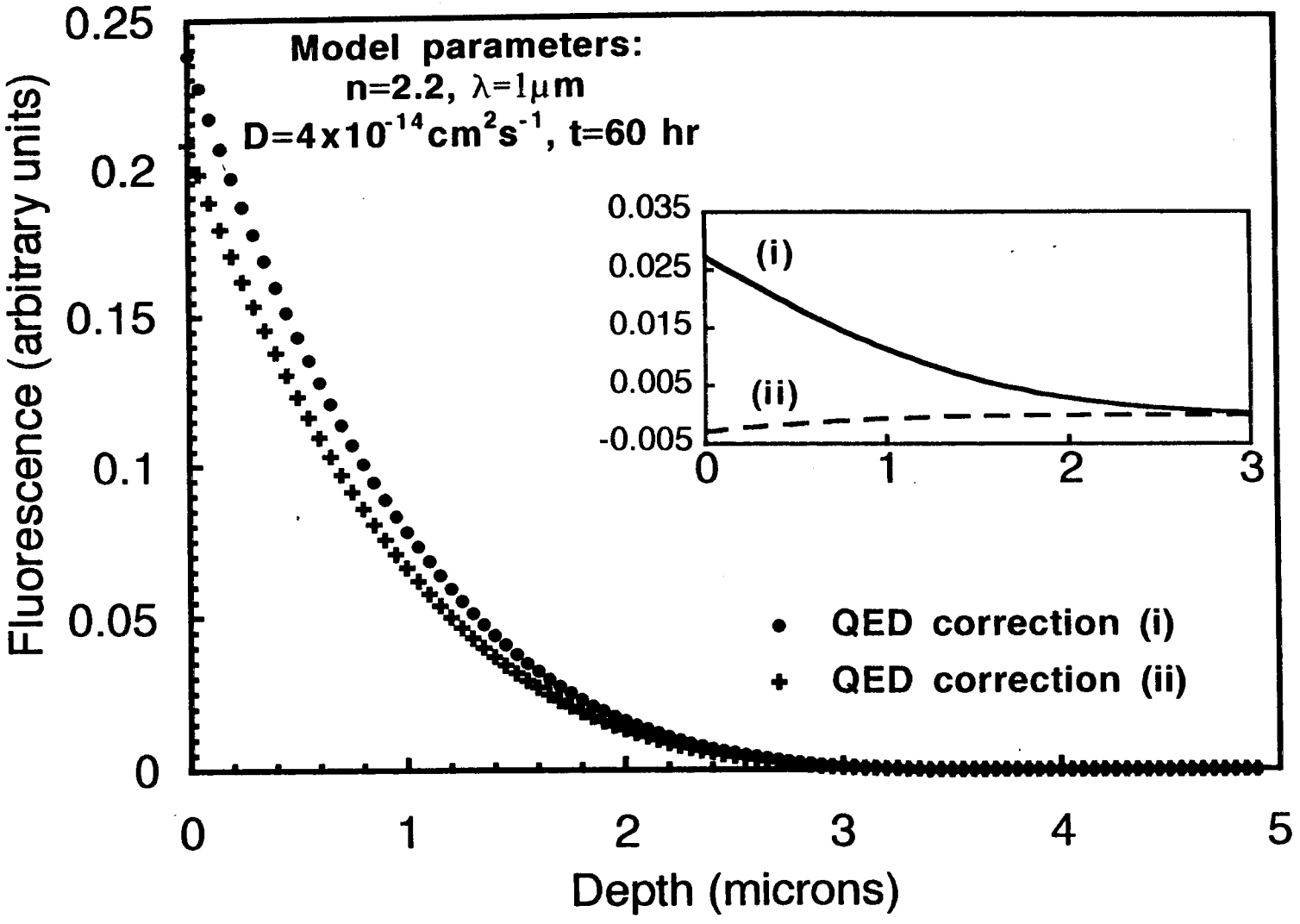
Model parameters:
n=2.2, λ=1μm
D=4x10^-14 cm^2 s^-1, t=60 hr
Fluorescence (arbitrary units)
Depth (microns)
0.25
0.2
0.15
0.1
0.05
0
0
1
2
3
4
5
0.035
0.025
0.015
0.005
-0.005
(i)
(ii)
QED correction (i)
QED correction (ii)

FIGURE 3

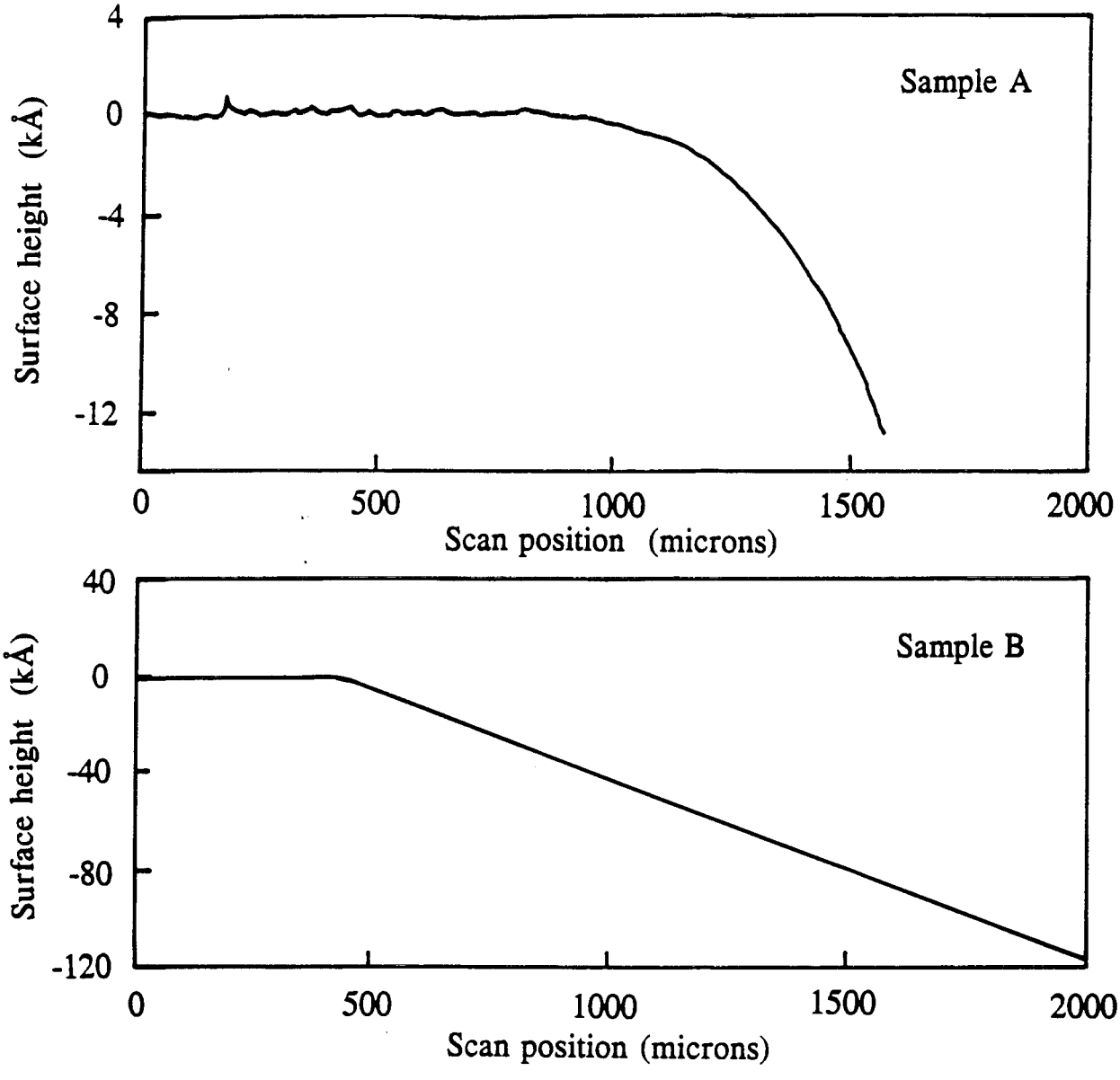
Sample A
Surface height (kÅ)
4
0
-4
-8
-12
0
500
1000
1500
2000
Scan position (microns)
Sample B
Surface height (kÅ)
40
0
-40
-80
-120
0
500
1000
1500
2000
Scan position (microns)

FIGURE 4

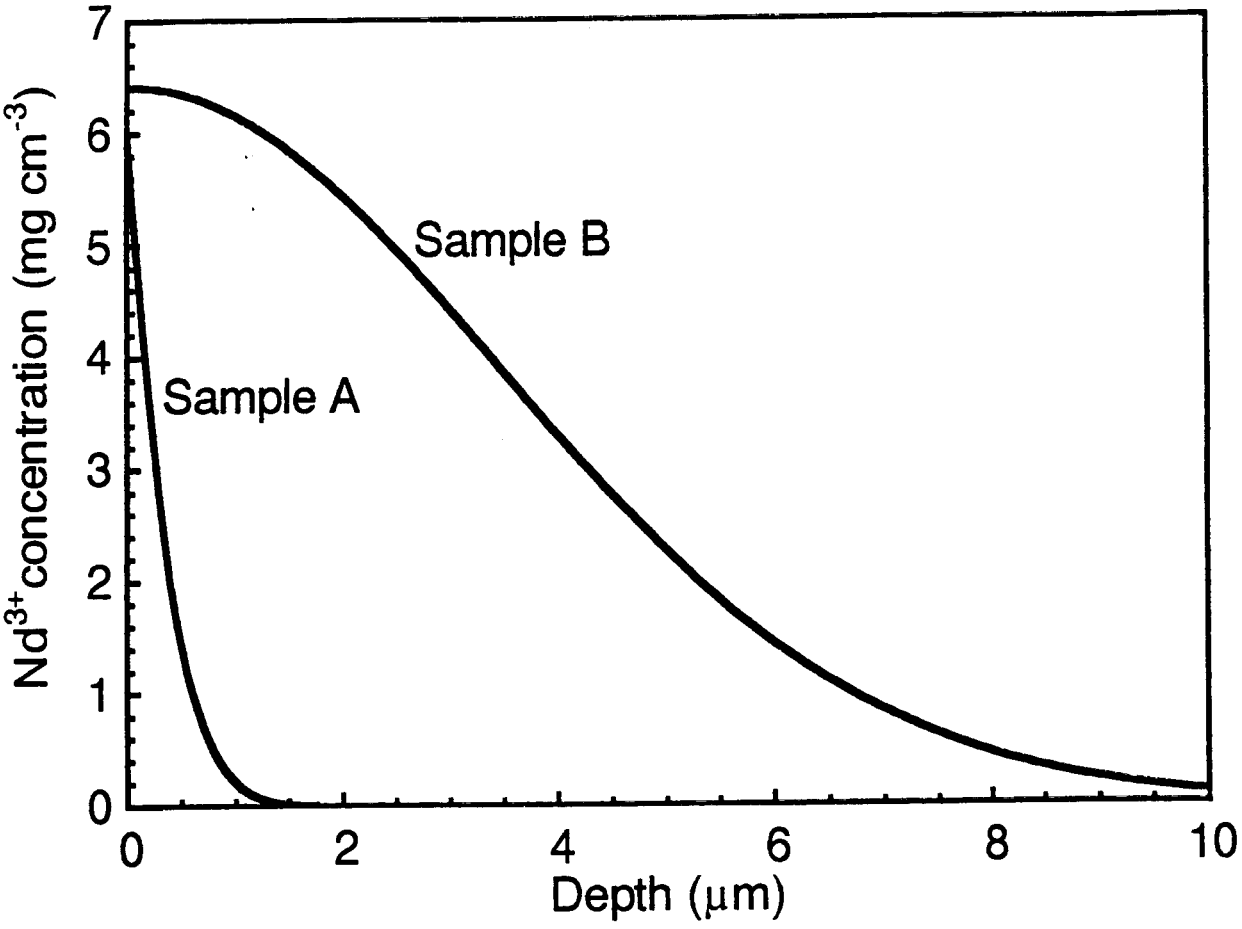
Nd3+concentration (mg cm-3)
Depth (μm)
Sample A
Sample B
0
1
2
3
4
5
6
7
0
2
4
6
8
10

FIGURE 5

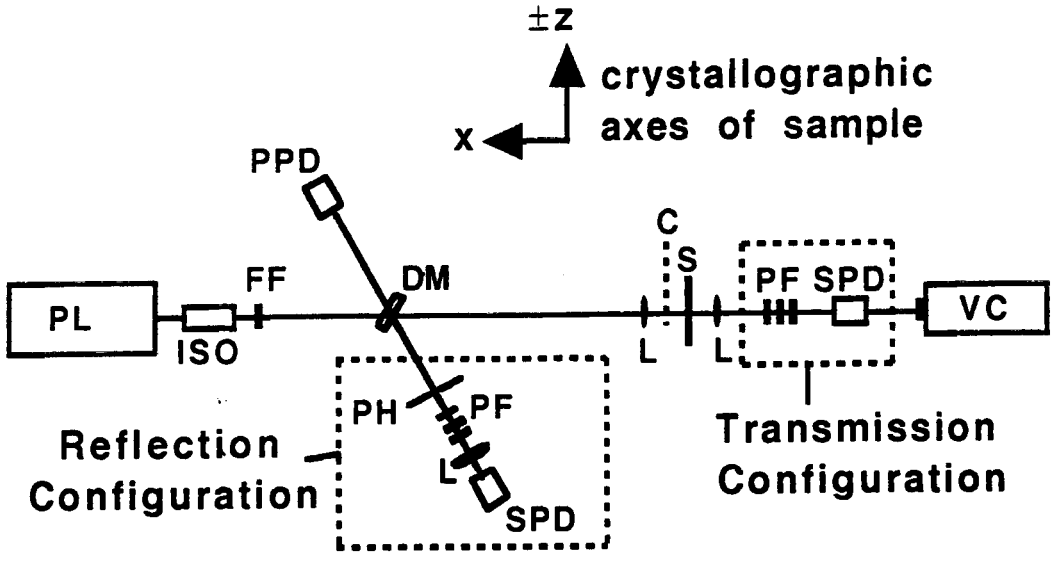
±z
crystallographic
axes of sample
x
PPD
C
S
PF SPD
PL
FF
DM
VC
ISO
L
L
PH
PF
L
SPD
Reflection
Configuration
Transmission
Configuration

FIGURE 6

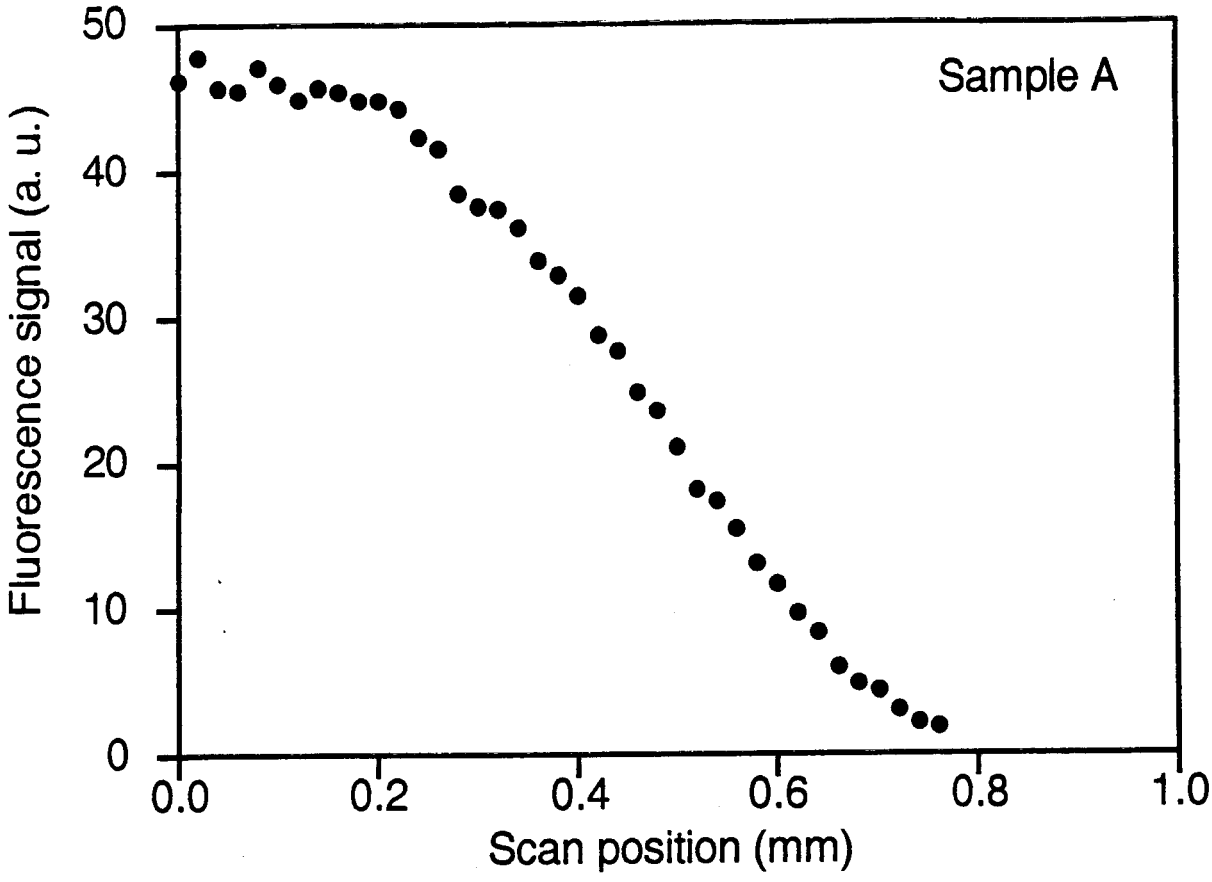
Sample A
Fluorescence signal (a. u.)
50
40
30
20
10
0
0.0
0.2
0.4
0.6
0.8
1.0
Scan position (mm)

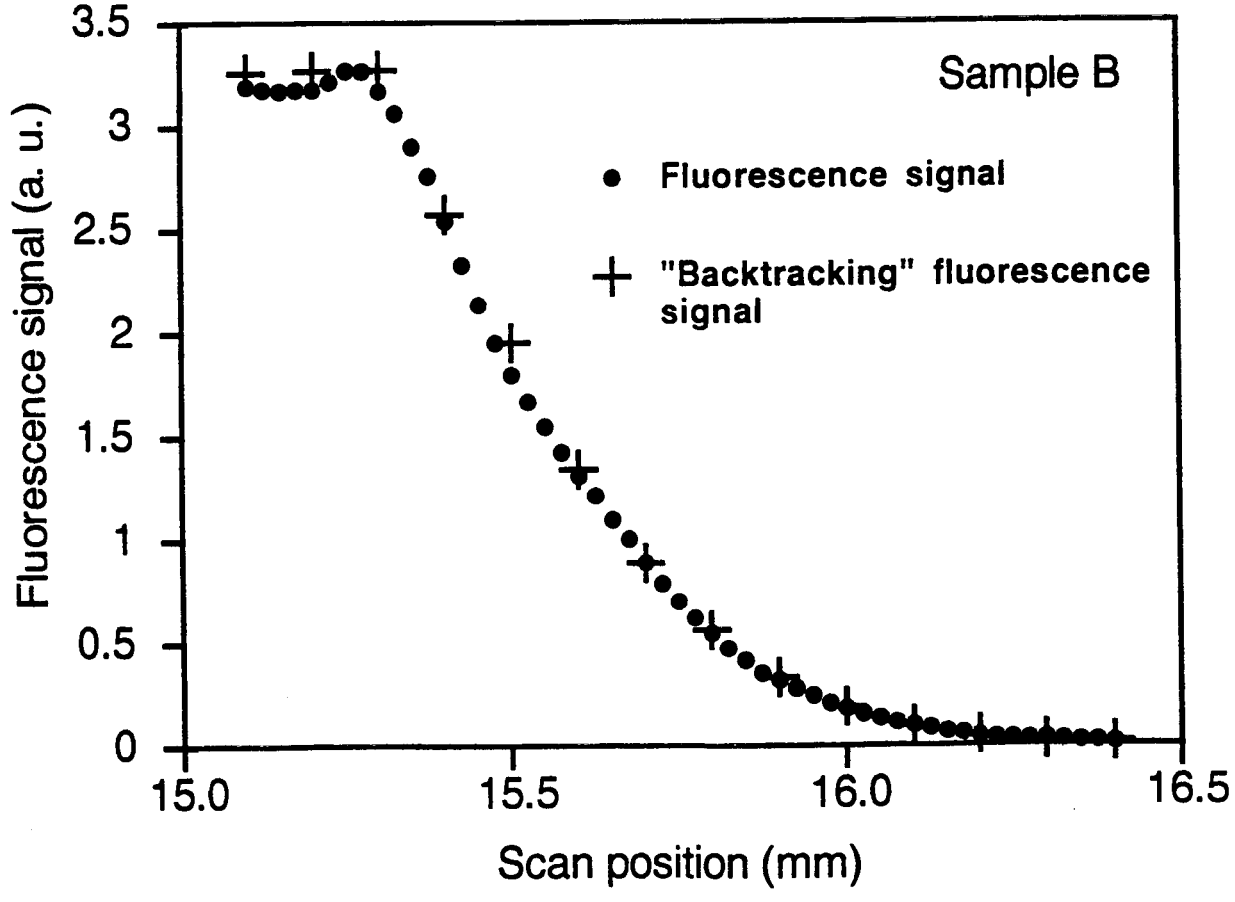
Sample B
Fluorescence signal
"Backtracking" fluorescence signal
Fluorescence signal (a. u.)
3.5
3
2.5
2
1.5
1
0.5
0
15.0
15.5
16.0
16.5
Scan position (mm)

FIGURE 7

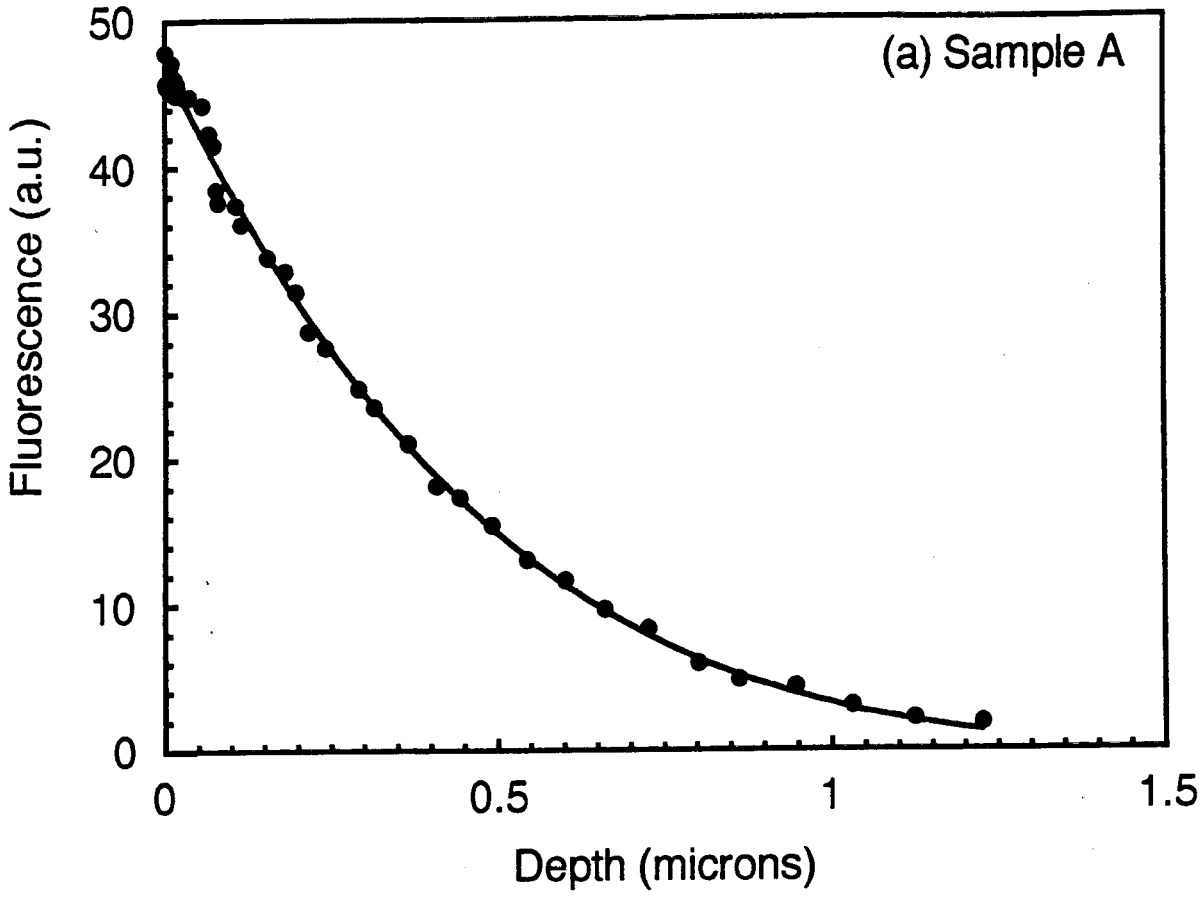
(a) Sample A
Fluorescence (a.u.)
50
40
30
20
10
0
0
0.5
1
1.5
Depth (microns)

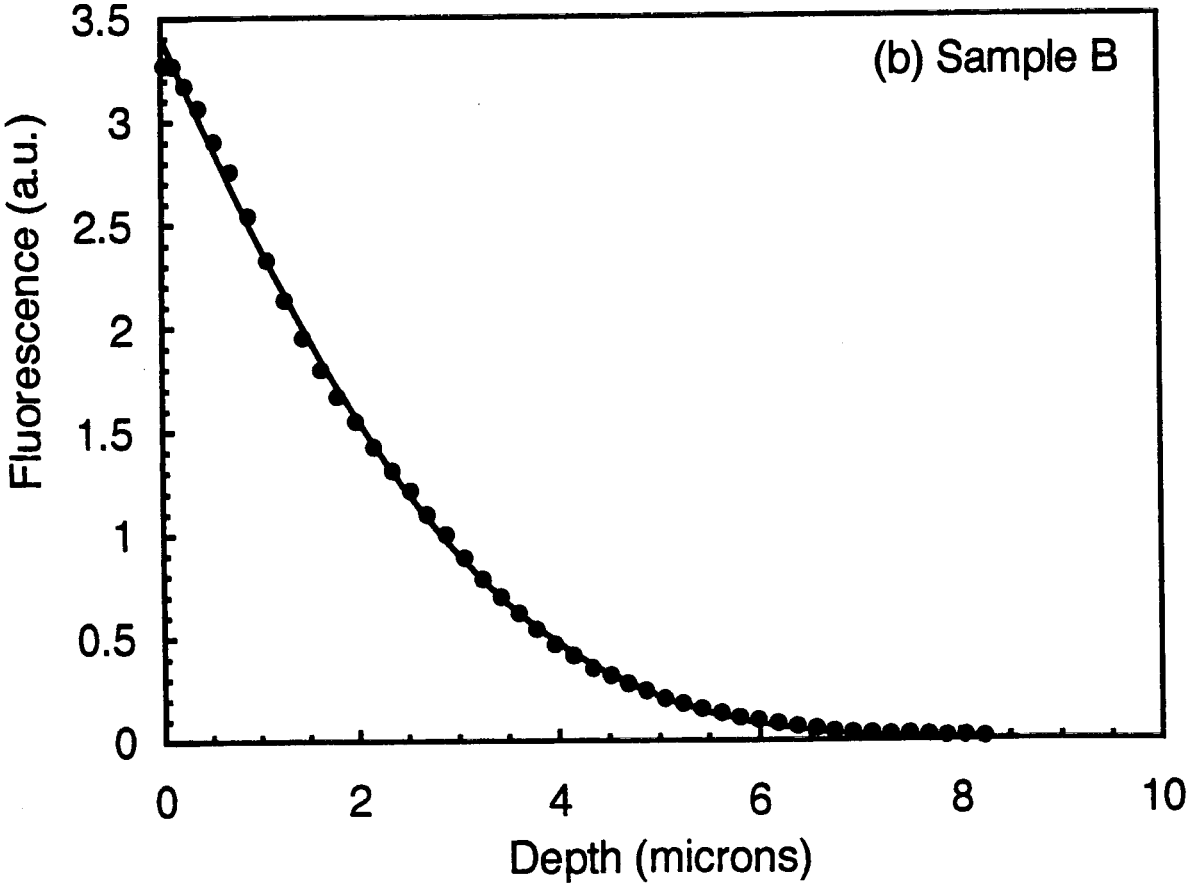
(b) Sample B
Fluorescence (a.u.)
3.5
3
2.5
2
1.5
1
0.5
0
0
2
4
6
8
10
Depth (microns)

FIGURE 8

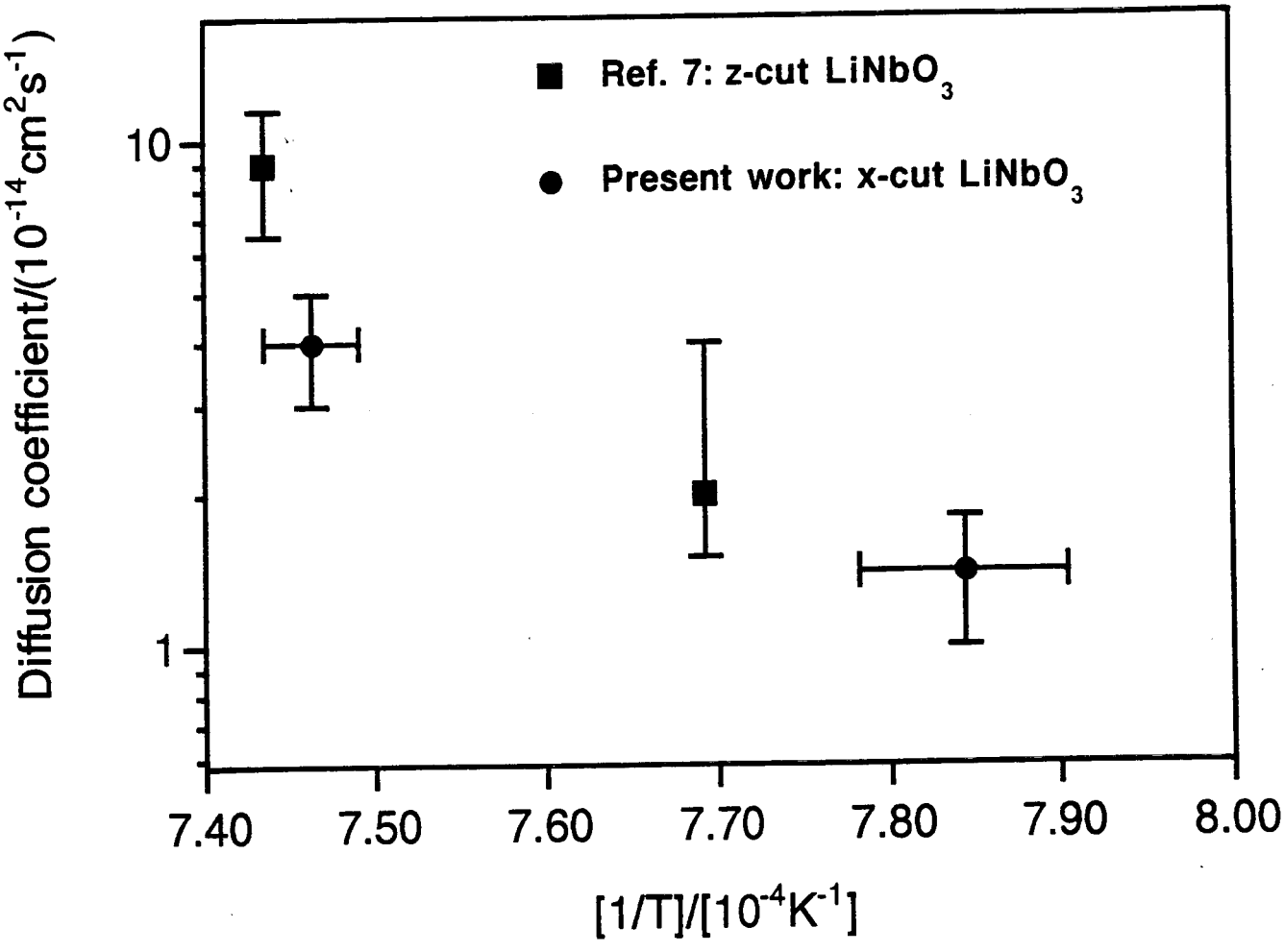
Diffusion coefficient/(10^-14 cm^2 s^-1)
10
1
Ref. 7: z-cut LiNbO3
Present work: x-cut LiNbO3
7.40
7.50
7.60
7.70
7.80
7.90
8.00
[1/T]/[10^-4 K^-1]

FIGURE 9

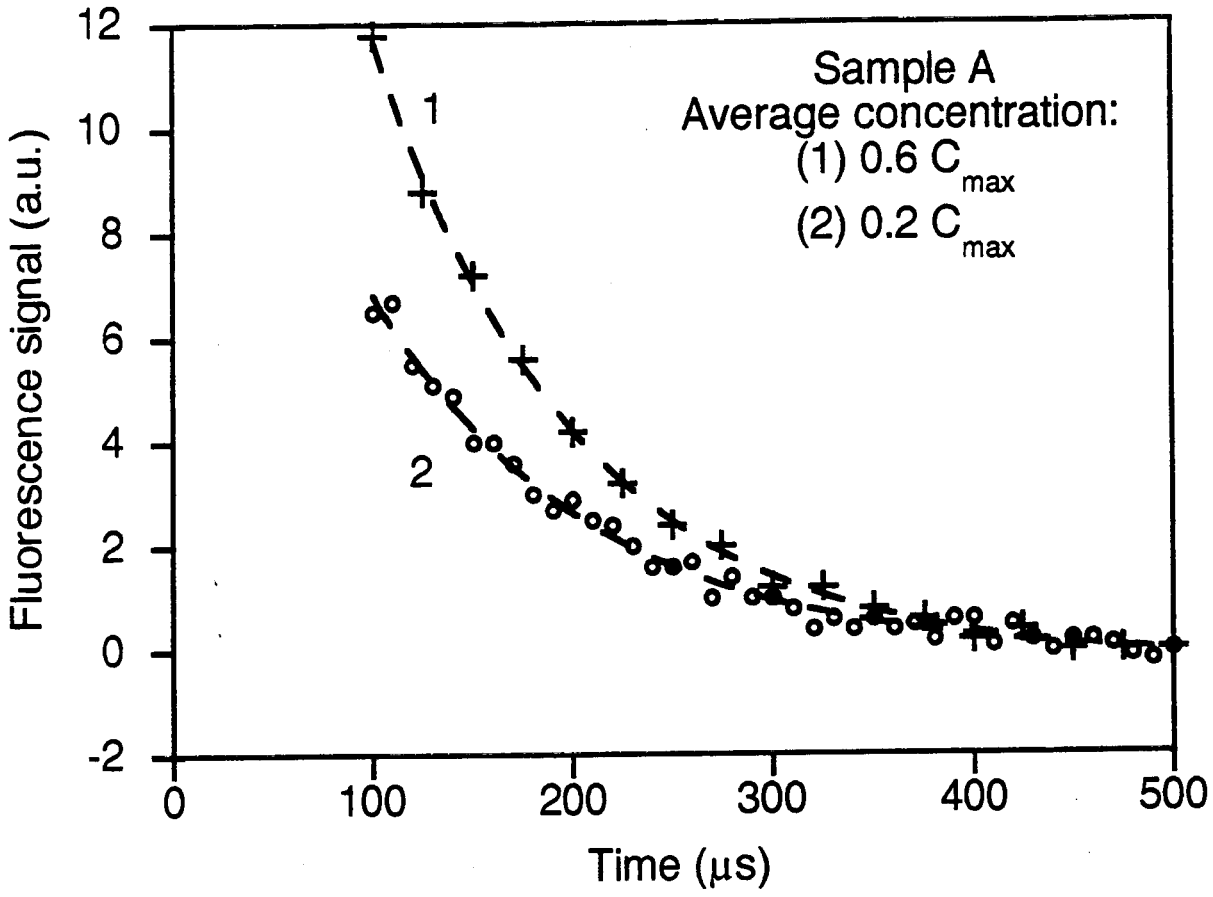
Sample A
Average concentration:
(1) 0.6 C max
(2) 0.2 C max
1
2
Fluorescence signal (a.u.)
Time (μs)
12
10
8
6
4
2
0
-2
0
100
200
300
400
500

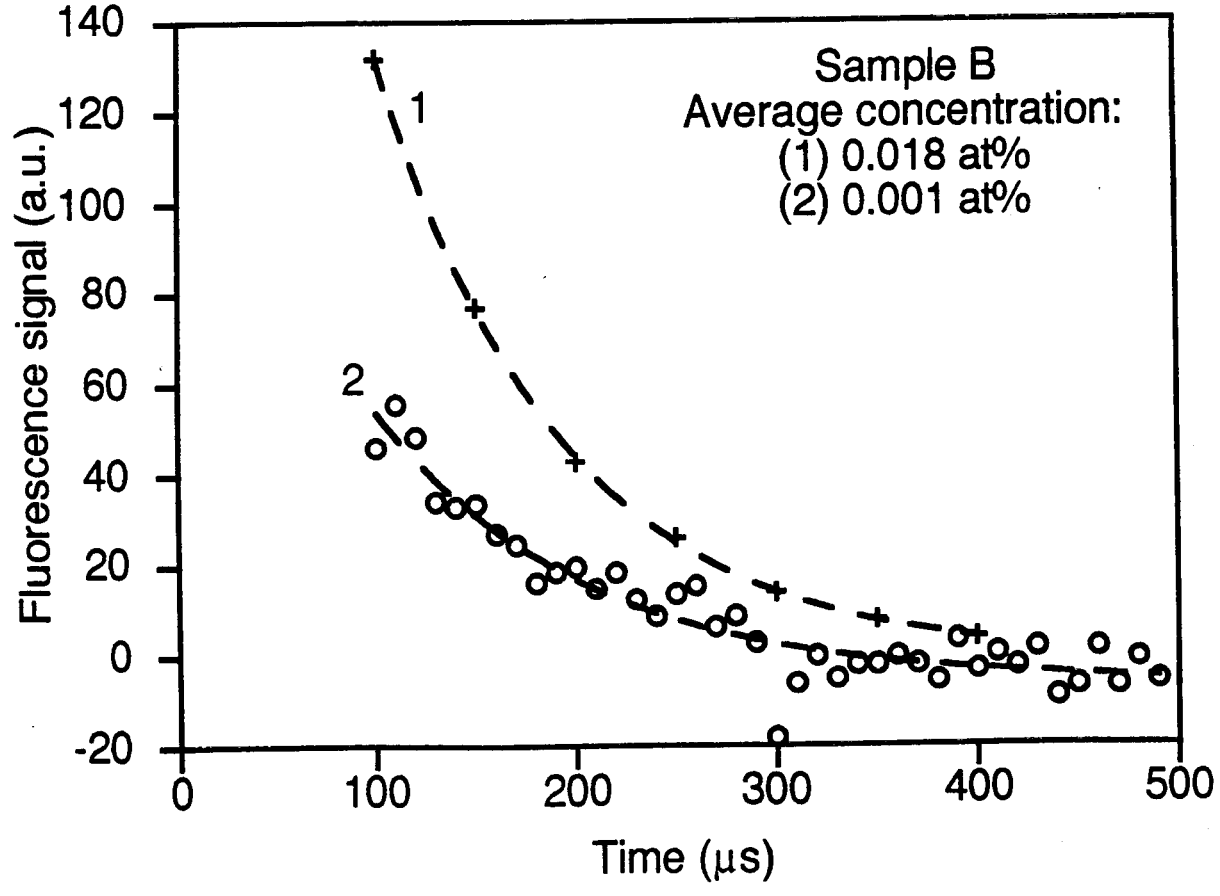
Sample B
Average concentration:
(1) 0.018 at%
(2) 0.001 at%
1
2
Fluorescence signal (a.u.)
Time (μs)
140
120
100
80
60
40
20
0
-20
0
100
200
300
400
500

FIGURE 10

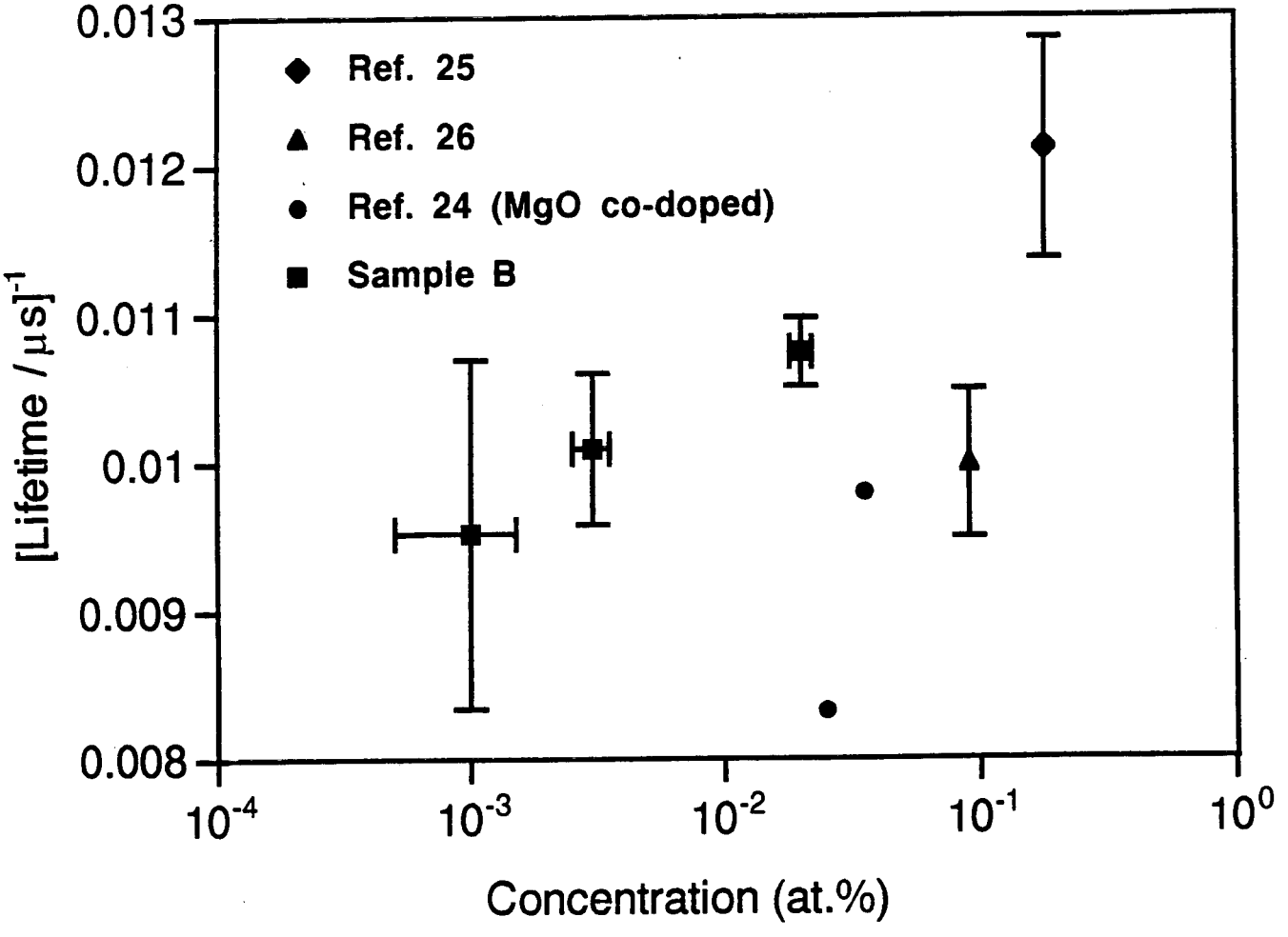
0.013
0.012
0.011
0.01
0.009
0.008
[Lifetime /μs]-1
Ref. 25
Ref. 26
Ref. 24 (MgO co-doped)
Sample B
10-4
10-3
10-2
10-1
100
Concentration (at.%)

FIGURE 11